Extraction of Anisotropic Contributions in Turbulent Flows

Itai Arad,[1] Brindesh Dhruva,[2] Susan Kurien,[1,2] Victor S. L'vov,[1,3] Itamar Procaccia,[1] and K. R. Sreenivasan[2]
[1]*Department of Chemical Physics, The Weizmann Institute of Science, Rehovot 76100, Israel*
[2]*Mason Laboratory and the Department of Physics, Yale University, New Haven, Connecticut 06520-8286*
[3]*Institute of Automatization and Electrometry Academy of Sciences of Russia, Novosibirsk 630090, Russia*
(Received 6 April 1998; revised manuscript received 9 September 1998)

We analyze turbulent velocity signals in the atmospheric surface layer, obtained by pairs of probes separated by inertial-range distances parallel to the ground and (nominally) orthogonal to the mean wind. The Taylor microscale Reynolds number ranges up to 20 000. Choosing a suitable coordinate system with respect to the mean wind, we derive theoretical forms for second order structure functions and fit them to experimental data. The effect of flow anisotropy is small for the longitudinal component but significant for the transverse component. The data provide an estimate for a universal exponent from among a hierarchy that governs the decay of flow anisotropy with the scale size. [S0031-9007(98)07959-9]

PACS numbers: 47.27.Gs, 05.40.+j, 47.27.Jv, 94.10.Jd

Experimental studies of turbulent flows at very high Reynolds numbers are usually limited in the sense that one measures the velocity field at a single spatial point as a function of time [1], and uses Taylor's hypothesis to identify velocity increments at different times with those across spatial length scales, R. The standard outputs of such measurements are the longitudinal two-point differences of the Eulerian velocity field and their moments, termed structure functions:

$$S_n(R) = \left\langle \left| [\mathbf{u}(\mathbf{r} + \mathbf{R}, t) - \mathbf{u}(\mathbf{r}, \mathbf{t})] \cdot \frac{\boldsymbol{R}}{R} \right|^n \right\rangle, \qquad (1)$$

where $\langle\cdot\rangle$ denotes averaging over time. In homogeneous and isotropic turbulence, these structure functions are observed to vary as a power law in R, $S_n(R) \sim R^{\zeta_n}$, with apparently universal scaling exponents ζ_n [2].

Recent progress in measurements [3] and in simulations [4] begins to offer information about the tensorial nature of structure functions. Ideally, one would like to measure the tensorial nth order structure functions defined as

$$\begin{aligned} S_n^{\alpha_1 \cdots \alpha_n}(\boldsymbol{R}) \equiv \langle & [u^{\alpha_1}(\boldsymbol{r} + \boldsymbol{R}) - u^{\alpha_1}(\boldsymbol{r})] \\ & \times [u^{\alpha_2}(\boldsymbol{r} + \boldsymbol{R}) - u^{\alpha_2}(\boldsymbol{r})] \\ & \cdots [u^{\alpha_n}(\boldsymbol{r} + \boldsymbol{R}) - u^{\alpha_n}(\boldsymbol{r})] \rangle, \end{aligned} \qquad (2)$$

where the superscript α_i indicates the velocity component in the direction i. Such information should be useful in studying the anisotropic effects induced by all practical means of forcing.

In analyzing experimental data the model of "homogeneous and isotropic small scale" is universally adopted, but it is important to examine the relevance of this model for realistic flows. One of the points of this Letter is that keeping the tensorial information helps significantly in disentangling different scaling contributions to structure functions [5]. Especially when anisotropy might lead to different scaling exponents for different tensorial components, a careful study of the various contributions is needed. We will show below that atmospheric measurements contain important anisotropic contributions to one type of transverse structure functions.

We analyze measurements in atmospheric turbulence at heights of 6 and 35 m above the ground (data sets I and II). Set I was acquired over a flat desert with a long fetch, and the Taylor microscale Reynolds number was about 10 000. Set II was acquired over a rough terrain with ill-defined fetch, and the microscale Reynolds number was 20 000 [6]. The data were acquired simultaneously from two single hot-wire probes separated by 55 cm (set I) and 40 cm (set II). In both cases, the separation distance was within the inertial range and was set nominally orthogonal to the mean wind direction (see below). The hot wires, about 0.7 mm in length and 6 μm in diameter, were calibrated just prior to mounting them on the meteorology towers and checked immediately after dismounting. The hot wires were operated on DISA 55M01 constant-temperature anemometers. The frequency response of the hot wires was typically good up to 20 kHz. The voltages from the anemometers were suitably low pass filtered and digitized. The voltages were constantly monitored on an oscilloscope to ensure that they did not exceed the digitizer limits. Also monitored on-line were spectra from an HP 3561A Dynamic Signal Analyzer. The wind speed and direction were independently monitored by a direction indicator mounted on the tower (set I) or a vane anemometer a few meters way (set II). The real-time durations of data records were limited only by the degree of constancy demanded of the wind speed and its direction. The Kolmogorov scales were about 0.75 mm (set I) and 0.45 mm (set II). Table I lists a few relevant facts about the data records analyzed here. The various symbols have the following meanings: $\overline{U}$ = local mean velocity, u' = root-mean-square velocity, $\langle\varepsilon\rangle$ = energy dissipation rate obtained by the assumption of local isotropy and Taylor's hypothesis, η and λ are the Kolmogorov and Taylor length scales, respectively, the microscale Reynolds number $R_\lambda \equiv u'\lambda/\nu$, and f_s is the sampling frequency.

 0031-9007/98/81(24)/5330(4)$15.00

TABLE I. Data sets I (first line) and II (second line).

$\overline{U}$ $\mathrm{m\,s^{-1}}$	u' $\mathrm{m\,s^{-1}}$	$10^2\langle\varepsilon\rangle$, $\mathrm{m^2\,s^{-3}}$	η mm	λ cm	R_λ	f_s, per channel, Hz	No. of samples
4.1	1.08	1.1	0.75	15	10 500	10 000	4×10^7
8.3	2.30	7.8	0.45	13	19 500	5 000	4×10^7

To test whether the separation between the two probes is indeed orthogonal to the mean wind, we computed the cross-correlation function $\langle u_1(t+\tau)u_2(t)\rangle$. Here, u_1 and u_2 refer to velocity fluctuations in the direction of the mean wind, for probes 1 and 2, respectively. If the separation were precisely orthogonal to the mean wind, this quantity should be maximum for $\tau = 0$. Instead, for set I, we found the maximum shifted slightly to $\tau = 0.022$ s, implying that the separation was not precisely orthogonal to the mean wind. To correct for this effect, the data from the second probe were time shifted by 0.022 s. This amounts to a change in the actual value of the orthogonal distance. We computed this effective distance to be $\Delta \approx 54$ cm (instead of the 55 cm that was set physically). For set II, the effective separation distance was estimated to be 31 cm (instead of the physically set 40 cm). Next we tested the isotropy of the flow for separations of the order of Δ. Define the "transverse" structure function across Δ as $S_T(\Delta) \equiv \langle[u_1(\bar{U}t) - u_2(\bar{U}t)]^2\rangle$ and the "longitudinal" structure function as $S_L(\Delta) \equiv \langle[u_1(\bar{U}t + \bar{U}t_\Delta) - u_1(\bar{U}t)]^2\rangle$, where $t_\Delta = \Delta/\bar{U}$. If the flow were isotropic we would expect [1]

$$S_T(\Delta) = S_L(\Delta) + \frac{\Delta}{2}\frac{\partial S_L(\Delta)}{\partial \Delta}. \tag{3}$$

In the isotropic state both components scale with the same exponent, $S_{T,L}(\Delta) \propto \Delta^{\zeta_2}$, and the ratio S_T/S_L is computed from (3) to be $1 + \zeta_2/2 \approx 1.35$, where $\zeta_2 \approx 0.69$ (see below). The experimental ratio was found to be 1.32 for set I, indicating that the anisotropy at the scale Δ is small. This same ratio was about 1.8 for set II, indicating a higher degree of anisotropy at that scale. The differences between the two data sets seem attributable at least partly to differences in the terrain and other atmospheric conditions.

To obtain a theoretical form of the structure function tensor we first select a natural coordinate system. An obvious choice is the mean-wind direction $\boldsymbol{n}$ along the 3-axis. The second axis is given by the separation vector $\boldsymbol{\Delta}$ between the two probes. We make the simplifying assumption of cylindrical symmetry about the mean-wind direction. It is shown *a posteriori* that this assumption probably accounts for most of the anisotropy *for this particular geometrical setup.*

To continue, we need to write down the tensor form for the general second order structure function [defined by Eq. (2) for $n = 2$] in terms of irreducible representations of the SO(3) rotation group. This tensor can be written in terms of the representations of the direct product of two three-dimensional Euclidean vector spaces (for the indices α, β) and the space of continuous functions on the unit sphere (for the direction of $\boldsymbol{R}$) [7]. The latter is spanned by the spherical harmonics $Y_{l,m}$, and the representations of the product space are indexed by j, denoting a $2j + 1$ dimensional irreducible representation. Every such representation is associated with a scalar function $c_j(R)$, which is expected to scale with a universal exponent $\zeta_2^{(j)}$; the exponent is an increasing function of j, and $\zeta_2^{(0)} = \zeta_2$. Previous theoretical considerations [8] led to the estimates $\zeta_2^{(1)} \approx 1, \zeta_2^{(2)} \approx 4/3$. We are interested in relatively modest anisotropies and so focus on the lowest order correction to the isotropic ($j = 0$) contribution. In other words, we write

$$S^{\alpha\beta}(\mathbf{R}) = S^{\alpha\beta}_{j=0}(\mathbf{R}) + S^{\alpha\beta}_{j=2}(\mathbf{R}) + \cdots. \tag{4}$$

We do not have a $j = 1$ term since the possible contributions to it vanish either because of parity considerations (the structure function itself is even in R) or by the incompressibility constraint. Now the most general form of the tensor can be written down by inspection. The case $j = 0$ is well known, and we write it as

$$S^{\alpha\beta}_{j=0}(\mathbf{R}) = c_0(R)\left[(2+\zeta_2)\delta^{\alpha\beta} - \zeta_2\frac{R^\alpha R^\beta}{R^2}\right], \tag{5}$$

where $c_0(R) = c_0 R^{\zeta_2}$, and c_0 is a nonuniversal numerical coefficient that needs to be obtained from fits to the data. The $j = 2$ component has six independent tensor forms and corresponding coefficients but can be simplified by imposing the conditions of incompressibility and orthogonality with the $j = 0$ part of the tensor. This leaves us (in the case of cylindrical symmetry) with two independent coefficients we call a and b, giving

$$\begin{aligned} S^{\alpha\beta}_{j=2}(\mathbf{R}) = {} & aR^{\zeta_2^{(2)}}\Big[(\zeta_2^{(2)}-2)\delta^{\alpha\beta} - \zeta_2^{(2)}(\zeta_2^{(2)}+6)\times\delta^{\alpha\beta}\frac{(\boldsymbol{n}\cdot\boldsymbol{R})^2}{R^2} + 2\zeta_2^{(2)}(\zeta_2^{(2)}-2)\frac{R^\alpha R^\beta(\boldsymbol{n}\cdot\boldsymbol{R})^2}{R^4} \\ & + ([\zeta_2^{(2)}]^2 + 3\zeta_2^{(2)} + 6)n^\alpha n^\beta - \frac{\zeta_2^{(2)}(\zeta_2^{(2)}-2)}{R^2}(R^\alpha n^\beta + R^\beta n^\alpha)(\boldsymbol{n}\cdot\boldsymbol{R})\Big] \\ & + bR^{\zeta_2^{(2)}}\Big[-(\zeta_2^{(2)}+3)(\zeta_2^{(2)}+2)\delta^{\alpha\beta}(\boldsymbol{n}\cdot\boldsymbol{R})^2 + (\zeta_2^{(2)}-2)\frac{R^\alpha R^\beta}{R^2} + (\zeta_2^{(2)}+3)(\zeta_2^{(2)}+2)n^\alpha n^\beta \\ & + (2\zeta_2^{(2)}+1)(\zeta_2^{(2)}-2)\frac{R^\alpha R^\beta(\boldsymbol{n}\cdot\boldsymbol{R})^2}{R^4} - ([\zeta_2^{(2)}]^2-4)(R^\alpha n^\beta + R^\beta n^\alpha)(\boldsymbol{n}\cdot\boldsymbol{R})\Big]. \end{aligned} \tag{6}$$

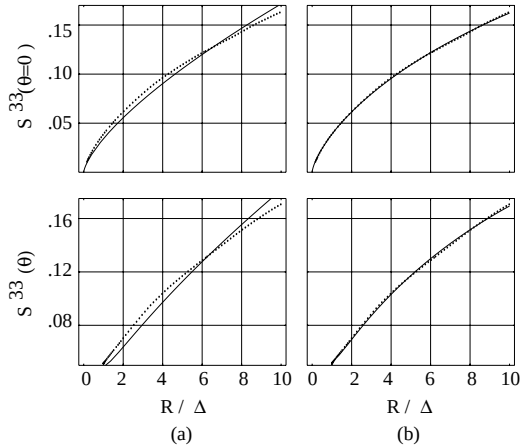

FIG. 1. The structure functions S^{33} for $\theta = 0$ and for nonzero θ computed for set I. The dots are for experimental data and the line is the analytic fit. Panel (a) presents fits to the $j = 0$ component only and panel (b) to components $j = 0$ and $j = 2$ together.

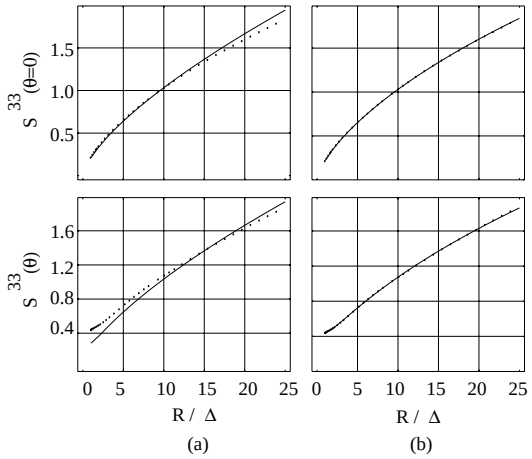

FIG. 2. The structure functions S^{33} for $\theta = 0$ and for nonzero θ computed for set II. The dots are for experimental data and the line is the analytic fit. Panel (a) presents fits to the $j = 0$ component only and panel (b) to components $j = 0$ and $j = 2$ together.

Finally, we note that in the present experimental setup only the component of the velocity in the direction of $\boldsymbol{n}$ is measured. In the coordinate system chosen above we can read from (6) the relevant component as

$$S^{33}(R,\theta) = S^{33}_{j=0}(R,\theta) + S^{33}_{j=2}(R,\theta) = c_0\left(\frac{R}{\Delta}\right)^{\zeta_2}[2 + \zeta_2 - \zeta_2\cos^2\theta] + a\left(\frac{R}{\Delta}\right)^{\zeta_2^{(2)}}$$
$$\times [(\zeta_2^{(2)} + 2)^2 - \zeta_2^{(2)}(3\zeta_2^{(2)} + 2)\cos^2\theta + 2\zeta_2^{(2)}(\zeta_2^{(2)} - 2)\cos^4\theta] + b\left(\frac{R}{\Delta}\right)^{\zeta_2^{(2)}}$$
$$\times [(\zeta_2^{(2)} + 2)(\zeta_2^{(2)} + 3) - \zeta_2^{(2)}(3\zeta_2^{(2)} + 4) \times \cos^2\theta + (2\zeta_2^{(2)} + 1)(\zeta_2^{(2)} - 2)\cos^4\theta]. \quad (7)$$

Here θ is the angle between $\boldsymbol{R}$ and $\boldsymbol{n}$, and R has been normalized by Δ, making all the coefficients dimensional, with units of $(\mathrm{m/sec})^2$. To fit these expressions to the experimental results we have converted, using Taylor's hypothesis [9], the structure functions computed from time differences for a single probe, and cross differences between the two probes. This allows us to obtain components of $S^{\alpha\beta}$ from (7), with $\theta = 0$ and variable, respectively. In other words,

$$S^{33}(R, \theta = 0) = \langle [u_1(\bar{U}t + \bar{U}t_R) - u_1(\bar{U}t)]^2 \rangle, \quad (8)$$

where $t_R \equiv R/\bar{U}$, and

$$S^{33}(R,\theta) = \langle [u_1(\bar{U}t + \bar{U}t_{\tilde{R}}) - u_2(\bar{U}t)]^2 \rangle. \quad (9)$$

Here $\theta = \arctan(\Delta/\bar{U}t_{\tilde{R}})$, $t_{\tilde{R}} = \tilde{R}/\bar{U}$, and $R = \sqrt{\Delta^2 + (\bar{U}t_{\tilde{R}})^2}$.

The quantities (8) and (9) computed from the experimental data were fitted to the theoretical expression (7) using the appropriate values of θ. The fits were performed in the range $1 < R/\Delta < 10$ (0.54 m $< R <$ 5.4 m) for set I and $1 < R/\Delta < 25$ (0.31 m $< R <$ 8 m). The ranges were based on the constancy of the third order structure function. Panels (a) of Figs. 1 and 2 show, for data sets I and II, respectively, a comparison between the measured $S^{33}(R, \theta = 0)$ and the $j = 0$ form of the equation. The comparison shows that the agreement is modest and that the best fit yields the exponent ζ_2 to be 0.69. To include the $j = 2$ contribution, we fixed ζ_2 to be 0.69 and performed the following analysis. For given values of the variables R and θ, we guessed the second exponent $\zeta_2^{(2)}$ and estimated the unknown coefficients c_0, a, and b by using a linear regression algorithm. We followed this procedure repeatedly for different values of $\zeta_2^{(2)}$ ranging from 0 to 2. We then chose the value of $\zeta_2^{(2)}$ that minimized χ^2 (the sum of the squares of the differences between the experimental data and the fitted values). The

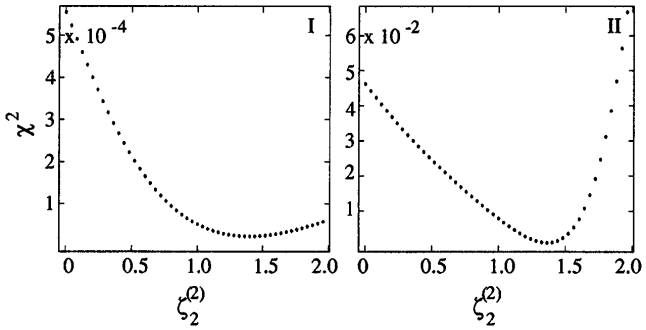

FIG. 3. The determination of the exponent $\zeta_2^{(2)}$ from a least-squares fit of $S^{33}(R,\theta)$ to its analytic form. From set I we obtain a numerical value of the best fit $\zeta_2^{(2)} = 1.38 \pm 0.15$, while from set II the best-fit value is 1.36 ± 0.1, both of which are in close agreement with the theoretical expectation of 4/3 (without intermittency corrections). The differences in the nature of the minima are not understood.

TABLE II. The scaling exponents and the three coefficients in units of $(\mathrm{m/sec})^2$ as determined from the nonlinear fit of Eq. (7) to data sets I (first line) and II (second line).

ζ_2	$\zeta_2^{(2)}$	c_0	a	b
0.69	1.38 ± 0.15	0.023 ± 0.001	−0.0051 ± 0.0006	0.0033 ± 0.0005
0.69	1.36 ± 0.10	0.112 ± 0.001	−0.052 ± 0.004	0.050 ± 0.004

corresponding values of the coefficients are chosen for further fitting purposes. For data set I, we found a "best-fit" value of the exponent from fitting only the values of $S^{33}(R,\theta=0)$. We then used this value of $\zeta_2^{(2)}$ in the expression for $S^{33}(R,\theta)$ in (7) and fit this to (9) to extract the coefficients c_0, a, and b. For data set II, we found the value of the exponent $\zeta_2^{(2)}$ by fitting simultaneously both $S^{33}(R,\theta=0)$ and $S^{33}(R,\theta)$.

In Fig. 3 we present χ^2 values as a function of $\zeta_2^{(2)}$. The optimal value of this exponent and the uncertainty determined from these plots is $\zeta_2^{(2)} \approx 1.38 \pm 0.15$ from set I and $\zeta_2^{(2)} \approx 1.36 \pm 0.1$ from set II. The best numerical values for the coefficients are presented in Table II. Panels (b) in Figs. 1 and 2 show the fits to the sum of $j=0$ and $j=2$ contributions to the experimental data. Even though the $j=2$ contributions are small, they improve the fits tremendously. This situation lends support to the essential correctness of the present analysis.

The figures show that the $\theta=0$ (purely longitudinal) structure function is somewhat less affected by the anisotropy than is the finite θ structure function (see especially Fig. 2). The reason is the closeness of the numerical absolute values of the coefficients a and b (see Table II). In the case $\theta=0$ the two tensor forms multiplied by a and b coincide, and the $j=2$ contribution becomes very small. The value of $\zeta_2=0.69$ quoted above can be obtained from such a fit to the $\zeta_2=0$ part alone; as long as one measures only this component, it seems reasonable to proceed with just that exponent. However, the inclusion of the second exponent $\zeta_2^{(2)}$ improves the fit even for the longitudinal case; for the finite θ case, this inclusion appears essential for a good fit [10].

To our knowledge, this determination of $\zeta_2^{(2)}$ is the first instance of finding an exponent describing the degree of anisotropy. The close agreement with the theoretical expectation of $4/3$ (e.g., Ref. [11]), and the apparent reproducibility of the result for two different experiments is a strong indication that this exponent is universal.

It should be understood that the exponents $\zeta_2^{(2)}$ (and also $\zeta_2^{(1)}$ that is unavailable from the present measurements) are just the smallest exponents in the hierarchy $\zeta_2^{(j)}$ that characterizes higher order irreducible representations indexed by j. The study of these exponents is in its infancy, and considerable experimental and theoretical effort is needed to reach firm conclusions regarding their universality and numerical values. We expect the exponents to be a nondecreasing function of j and that the highest values of j are being peeled off quickly when R decreases. Nevertheless, the lower order values of $\zeta_2^{(j)}$ can be measured and computed. We intend to proceed in this direction.

At Weizmann, the work was supported by the Basic Research Fund administered by the Israeli Academy of Sciences, the U.S.-Israel Binational Science Foundation, and the Naftali and Anna Backenroth-Bronicki Fund for Research in Chaos and Complexity. At Yale, it was supported by National Science Foundation Grant No. DMR-95-29609 and the Yale-Weizmann Exchange Program. Special thanks are due Dr. Yoshiyuki Tsuji, Mr. Christopher White, and Mr. Victor Cassella for their help in acquiring the data.

[1] A. S. Monin and A. M. Yaglom, *Statistical Fluid Mechanics* (MIT, Cambridge, 1971), Vol. 2.

[2] U. Frisch, *Turbulence: The Legacy of A. N. Kolmogorov* (Cambridge University Press, Cambridge, England, 1995); N. Cao, S. Chen, and Z.-S. She, Phys. Rev. Lett. **76**, 3711 (1996).

[3] R. Camussi, D. Barbagallo, G. Guj, and F. Stella, Phys. Fluids **8**, 1181 (1996); A. Noullez, G. Wallace, W. Lempert, R. B. Miles, and U. Frisch, J. Fluid Mech. **339**, 287 (1997); B. Dhruva, Y. Tsuji, and K. R. Sreenivasan, Phys. Rev. E **56**, R4928 (1997).

[4] O. M. Boratav, Phys. Fluids **339**, 287 (1997); S. Chen, K. R. Sreenivasan, M. Nelkin, and N. Cao, Phys. Rev. Lett. **79**, 2253 (1997).

[5] V. S. L'vov, E. Podivilov, and I. Procaccia, Phys. Rev. Lett. **79**, 2050 (1997); S. Grossmann, D. Lohse, and A. Reeh, J. Stat. Phys. (to be published).

[6] K. R. Sreenivasan and B. Dhruva, Prog. Theo. Phys. **130**, 103 (1998).

[7] I. Arad, V. S. L'vov, and I. Procaccia (to be published).

[8] D. C. Leslie, *Developments in the Theory of Turbulence* (Claredon Press, Oxford, 1973); S. Grossmann, D. Lohse, V. L'vov, and I. Procaccia, Phys. Rev. Lett. **73**, 432 (1994); E. A. Kuznetsov and V. S. L'vov, Physica (Amsterdam) **2D**, 203 (1981).

[9] To assess the effects of high turbulence level on Taylor's hypothesis, we compared structure functions of two signals with turbulence levels differing by a factor of 2 and found no difference. The correction scheme of G. Stolovitzky (Ph.D. thesis, Yale University, 1994) also showed no changes. For a few separation distances, the statistics of velocity increments from two probes separated along **n** agreed with Taylor's hypothesis.

[10] In fact, the fit using $j=0$ and $j=2$ for data set II extends all the way to 40 m (not shown in Fig. 2). This indicates that the "inertial range" where scaling theory applies is much longer than anticipated by traditional log-log plots.

[11] J. L. Lumley, Phys. Fluids **10**, 855 (1967).